Oxidation of Cyclohexane by a High-Valent Iron Bispidine Complex: A Combined Experimental and Computational Mechanistic Study†

Peter Comba,* Martin Maurer, and Prabha Vadivelu

Universität Heidelberg, Anorganisch-Chemisches Institut, INF 270, D-69120 Heidelberg, Germany

Received: April 30, 2008; Revised Manuscript Received: July 25, 2008

Experimental data suggest that there are various competing pathways for the catalytic and stoichiometric oxygenation of cyclohexane, assisted by iron-bispidine complexes and using various oxidants (H_2O_2, O_2, PhIO). Density functional theory calculations indicate that both Fe^{IV}=O and Fe^{V}=O species are accessible and efficiently transfer their oxygen atoms to cyclohexane. The reactivities of the two isomers each and the two possible spin states for the Fe^{IV}=O and Fe^{V}=O species are sufficiently different to allow an interpretation of the experimental data.

Introduction

Mononuclear nonheme iron enzymes are involved in a wide range of biological processes, where the initial step is dioxygen activation.[1,2] Thorough studies of biological systems have focused on clarifying the catalytic pathways in these enzymes,[3] and much experimental effort has been devoted to investigating the catalytic activity of low molecular weight model complexes.[4] In the hydroxylation of alkanes, there is an ongoing debate on the type of catalytically active oxidant, that is, Fe^{IV}=O, Fe^{V}=O, or oxygen-based radicals.[5−10] With the tetradentate tpa ligand (tpa = tris(2-pyridylmethyl)amine), it was shown that $[(tpa)Fe^{V}=O(OH)]^{2+}$, derived from O−O bond heterolysis of its $[(tpa)Fe_2^{III}(OOH)(OH_2)]^{2+}$ precursor, is the oxidant for alkane hydroxylation.[5,6] In contrast, fully characterized Fe^{IV}=O complexes with tetradentate N_4 ligands such as tmc (tmc = 1,4,8,11-tetramethylcyclam) and pentatendate ligands such as N4py (N4py = *N*,*N*-bis(2-pyridylmethyl)-bis(2-pyridyl)methylamine) and bpmen (bpmen = *N*-benzyl-*N*,*N*′,*N*′-tris(2-pridylmethyl)-1,2-diaminoethane) were shown to catalytically oxidize alkenes.[7,11] It was demonstrated that the pentatendate ligand Fe^{IV}=O complexes have longer life times than the ferryl species of tetradentate ligands and that they are thermally more stable.[7] This allowed the pentadentate ligand ferryl complexes to hydroxylate even the more inert alkanes, for example, cyclohexane, which has a C−H bond energy of 416 kJ/mol. In support for the Fe^{IV} route, direct spectroscopic evidence for a ferryl intermediate has been reported for the 2-oxoglutarate-dependent enzyme TauD.[12,13]

A similar debate on the active oxidant emerges from theoretical studies. Dioxygen activation was studied both via homolytic and via heterolytic pathways.[14] It was shown that, for the hydrogen-peroxide-derived $[(tpa)Fe^{III}(OOH)(OH_2)]^{2+}$ complex, the heterolytic pathway leading to Fe^{V}=O is preferred over the homolytic O−O bond cleavage, whereas for the reaction with alkyl peroxide, the homolytic pathway leading to an Fe^{IV}=O oxidant is preferred. The difference between hydrogen peroxide and alkyl peroxide as oxidant derives from the 33.5 kJ/mol higher O−O bond energy of hydrogen peroxide. In another density functional theory (DFT)-based study, supported by experiments and based on Fe^{II} complexes of tetradentate bispidine ligands (bispidines are rigid amine/pyridine ligands; see Figure 1), three pathways for the formation of the active catalyst from the Fe^{II} precatalyst were studied in detail.[15] One leads to Fe^{V}=O via an Fe^{III} intermediate, and the other two produce Fe^{IV}=O ferryl complexes. It followed that the direct conversion of Fe^{II} to Fe^{IV} is the preferred route, and the ferryl complexes were shown by DFT and by experiment to be efficient oxidants for alkenes.[16]

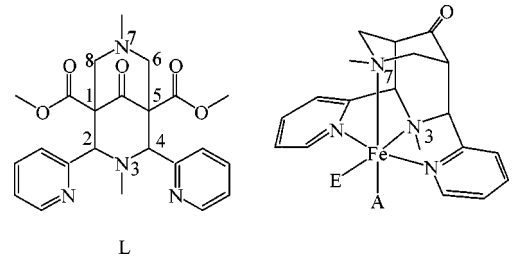

Figure 1. Tetradentate bispidine ligand L and its hexacoordinate Fe complex with an axial (A) and an equatorial (E) coligand; there are two isomeric oxo complexes with O as the axial ligand (*1*,*2*$_{transN7}$, O = A) or with O as the equatorial ligand (*1*,*2*$_{transN3}$, O = E).

Generally, the mechanism for iron-catalyzed alkane hydroxylation can be separated into two components, a C−H bond cleavage and a C−O bond formation step (see eq 1). At one extreme, the two steps may occur in a concerted fashion; that is, the oxygen atom is formally inserted into the C−H bond, or the C−H bond is cleaved to form an alkyl radical, which then is immediately trapped to form the C−O bond. Such a concerted mechanism was observed for the cytochrome P450 and methane monooxygenase (MMO) enzymes.[17,18] At the other extreme, the two steps (C−H cleavage and reaction of the resulting radical) are well-separated in time, so that the long-lived alkyl radical can be trapped by other species in solution. For example, Fe(BLM) (BLM = bleomycine) affords distinct DNA oxidation products that depend on the presence or absence of O_2.[19−21] Therefore, the lifetime of the nascent alkyl radical and its consecutive reactions are symptomatic for the type of mechanism involved.

$$R-H + Fe=O \rightarrow R^{\bullet} + Fe-OH \rightarrow R-OH + Fe \quad (1)$$

Another important aspect is the type of oxidant in the initial step of the alkane hydroxylation, that is, whether it is a metal-

† Part of the "Sason S. Shaik Festschrift".

* Corresponding author. Fax: +49-6226-546617. E-mail: peter.comba@aci.uni-heidelberg.de.

10.1021/jp8037895 CCC: $40.75
Published on Web 09/23/2008

based oxidant (and if so in which oxidation state the iron center is) or an O-based radical (OH• or OR•). The former, for example, in cytochrome P450 and MMO, produces short-lived alkyl radicals; the latter leads to longer-lived alkyl radicals, which diffuse freely in solution, and in the presence of O_2, a radical chain oxidation may be initiated. The alcohol/ketone ratio (a/k) reflects the lifetime of the alkyl radical to some extent. With long-lived alkyl radicals of secondary alkanes such as cyclohexane, these are trapped by O_2 to produce alkylperoxyl radicals,[22] which in a Russell-type termination step yield equimolar amounts of alcohol and ketone.[23] Alkyl radicals formed by metal-based oxidants react quickly with the metal center in the oxygen rebound mechanism,[24] and this has an estimated rate constant of $10^{10}\sim10^{13}$ s^{-1}.[25,26] Alcohols are expected to be the only product of the rebound process, but ketones may also be observed because of the further oxidation of the alcohol product.

Well-studied nonheme iron model systems are those of the tetradentate pyridine-based ligands $[Fe(tpa)(NCCH_3)_2]^{2+}$ and $[Fe(bpmen)(NCCH_3)_2]^{2+}$.[27,28] Both are efficient catalyst systems with 40−70% of H_2O_2 converted to the products. The high a/k ratios are independent of the presence of O_2, and high kinetic isotope effects (KIE > 3) for the cyclohexane oxidation indicate that the mechanism involves a metal-based oxidant and short-lived alkyl radicals. The reaction with the closely related pentadentate ligand catalyst $[Fe(N4py)(NCCH_3)]^{2+}$ shows a significantly different reactivity pattern; the oxidation of cyclohexane is accompanied by a KIE of only 1.5 and a low a/k ratio (1.4), which also varies in the presence of O_2.[29,30] This suggests that hydroxyl radicals and long-lived alkyl radicals play an important role in these reactions. From the observed reactivity pattern, the decomposition of $[Fe(tpa)(OOH)]^{3+}$ appears to result in O−O bond heterolysis, with no OH• radicals involved and leading to an Fe^{V}═O oxidant. This pathway is excluded by the reactivity patterns of the pentadentate ligand system. It was concluded that the presence of two labile sites on the metal center is a key feature for the reactivity of the $[Fe(tpa)(NCCH_3)_2]^{2+}$ and $[Fe(bpmen)(NCCH_3)_2]^{2+}$ systems.

Here, we report a combined experimental and computational study of an Fe^{II}-based catalyst system with a tetradentate bispidine ligand (see Figure 1). The focus is on the computational part of the study, and particular emphasis is put on the thermodynamics and kinetics of the formation and the reactivity of the Fe^{IV}═O and Fe^{V}═O complexes in all possible spin states.

Experimental Section

Oxidation Experiments. The bispidine ligand L and the corresponding iron(II) complexes were prepared as described before.[31] Typical conditions for the oxidation of cyclohexane are given here for the reaction with H_2O_2 as oxidant (there are small differences dependent on the oxidant and the type of reaction, i.e. stoichiometric or catalytic, ambient or anaerobic atmosphere). A 30% aqueous solution of H_2O_2 (210 μmol) was slowly added (over 30 min) via a syringe pump to a solution of cyclohexane (2.1 mmol) and the catalyst (2.1 μmol) in MeCN (3 mL) at 25 °C. The solution was stirred for 5 min after the addition of H_2O_2 was complete. All product mixtures were filtered over a short silica plug before GC analysis on a Varian 3900 instrument, equipped with a ZB-1701 column. The products were quantified relative to naphthalene as internal standard.

Computational Details. All calculations were performed with DFT, using the Jaguar 6.5 program package.[32] The B3LYP functional[33−35] and LACVP basis set (double ζ, with a Los Alamos effective core potential for the Fe center, and 6−31G for the other atoms) were used.[36,37] The geometry optimization with this basis allows a pseudo-spectral optimization algorithm, and as a result, the calculations are robust even with relatively large molecules.[38] All intermediates were confirmed by frequency calculations as minima on the potential energy surface, and this was done with Gaussian 03.[32,39] To obtain reliable energetics, single point calculations were performed on the B3LYP/LACVP-optimized geometries, using the LACV3P++** basis set (LanL2DZ on the Fe center and 6−311++G** on the remaining atoms). The quoted energies are those calculated at the B3LYP/LACV3P++** level and include zero point and free energy corrections (the latter two are derived from the B3LYP/LACVP calculations). Single point calculations on the B3LYP/LACVP geometries were also performed with the polarized continuum model (PCM)[40−43] with acetonitrile as solvent. Differences due to solvation are minimal (<±15 kJ/mol), and they do not affect the trend to that obtained at the B3LYP/LACVP level. The effects of MeCN as solvent are therefore neglected in the data discussed here.

Results and Discussion

Cyclohexane Hydroxylation Experiments. The activity of the Fe^{II} complex of the tetradentate bispidine ligand L, $[(L)Fe^{II}(solvent)_2]^{2+}$ (see Figure 1), for the oxidation of cyclohexane with O_2, H_2O_2, and iodosyl benzene (PhIO) was examined, and the experimental results are summarized in Table 1. Note that, in contrast to most other model studies discussed in the introduction, the precatalyst is in the +II oxidation state and a high-spin electronic configuration (the corresponding Fe^{III} complexes are generally less stable). The standard conditions used are MeCN solutions (3 mL) at 25 °C, anaerobic environment (Ar), 30 min reaction time and catalyst/oxidant/substrate (cyclohexane) ratios of 1:100:1000 in the catalytic reactions or 1.0 equivalent of the oxidant and a 100-fold excess of the substrate in the stoichiometric reactions. The catalytic oxidation of cyclohexane, using $[(L)Fe^{II}(solvent)_2]^{2+}$ as precatalyst and H_2O_2 as oxidant, yields 34 turnovers (entry 1; maximum of 100 turnovers, i.e. a yield of approximately 35%) with a 4:3 excess of alcohol over ketone product, and these are reactivities and selectivities which are between those of the tpa- and N4py-based iron catalyst systems. That is, metal-based oxidants seem to be of importance, but pathways based on hydroxyl radicals and autoxidation might also be involved. Iodosyl benzene was therefore used as an alternative oxidant because PhIO is known to selectively form $[(L)Fe^{IV}$═$O(solvent)]^{2+}$, while H_2O_2 may lead to active Fe^{IV} and Fe^{V} species.[15] Interestingly, the reaction

TABLE 1: Experimentally Observed Products of the Iron-Bispidine-Catalyzed Oxidation of Cyclohexane

entry	experimental conditions[a]	alcohol[b]	ketone[b]
1	H_2O_2, argon	20	14
2	H_2O_2, air	13	12
3	O_2 from air (18 h)	1	3.5
4	PhIO, argon (18 h)	0.9	1
5	PhIO[c], argon	16%	4.5%
6	PhIO[c], air	26%	15%
7	PhIO[c,d], argon	0%	0%
8	PhIO[c,d], air	0%	0%

[a] 1000 eq. cyclohexane/100 eq. oxidant/1eq. catalyst; reaction time of 35 min, CH_3CN 298 K (unless otherwise specified). [b] For catalytic reactions: TON = mol product per mol catalyst; for stoichiometric reactions: % yield. [c] Stoichiometric reaction (1.0 eq. oxidant; 100-fold excess of substrate). [d] MeOH as solvent.

of $[(L)Fe^{II}(solvent)_2]^{2+}$ with PhIO did not show a significant catalytic activity (entry 4), but in a stoichiometric reaction, cyclohexane is oxidized by the Fe^{II}/PhIO system, primarily to cyclohexanol in up to 40% overall yield (entries 5,6). The difference in the a/k ratio between the H_2O_2 and the PhIO reactions (entry 1 vs entry 5) indicates that there are different pathways involved, for example, Fe^{V} versus Fe^{IV}. The increasing yield in the presence of O_2 (a/k of approximately 1:1, entry 5 vs entry 6) indicates a significant lifetime of the cyclohexyl radical. This shows that $[(L)Fe^{IV}{=}O(solvent)]^{2+}$ is an active oxidant; possible reasons for the lack of catalytic activity are that the catalytic cycle with H_2O_2 as oxidant follows another pathway (e.g., involving $Fe^{V}{=}O$) or that the product (cyclohexanol) inhibits the catalysis under the conditions used in the PhIO experiments. To test the latter possibility (inhibition by alcohols), MeOH was also used as solvent instead of MeCN in the stoichiometric reaction with PhIO (entries 7,8). The oxidation of cyclohexane to cyclohexanol ceases when MeCN is substituted by MeOH. Whether this means that alcohols (including cyclohexanol) inhibit the oxidation reaction or that MeCN (coordinated to the iron center) is required in the catalytic cycle cannot be decided on the basis of the current experimental data.

Altogether, the experimental data are not unambiguous with respect to the assignment of mechanistic pathways. It is clear that more experimental data are needed for a more thorough analysis, and this will be reported elsewhere in due course. The general conclusions from the experimental data from Table 1 and the basis for the computational study are as follows. The pathways using H_2O_2 and PhIO as oxidants are clearly different. Specifically, it appears that the PhIO oxidation, leading to $Fe^{IV}{=}O$, produces a cyclohexyl radical of significant lifetime (auto-oxidation at ambient atmosphere; entries 5,6), and this does not seem to be the case with H_2O_2 as oxidant (entries 1,2). The stoichiometric reactions with PhIO as oxidant and MeOH as solvent (entries 7,8) seem to confirm that alcohols inhibit the catalytic oxygen transfer (see entry 4). However, MeOH is also known to trap radicals. Therefore, an interpretation of the solvent dependence observed here is not unambiguous with the limited amount of experimental data.

Because of ambiguities emerging from the experimental data, DFT calculations are used to further elucidate the catalytic pathway. The computational studies involve the usual putative intermediates and transition states (hydrogen abstraction to a radical intermediate, followed by a radical rebound process) in all possible spin states and including the $[(L)Fe^{IV}{=}O(OH)]^{+}$ and the $[(L)Fe^{V}{=}O(OH)]^{2+}$ species as possible oxidants.[1,2,4,5] The methods used are those used before for the computational analysis of high-valent iron-bispidine systems, where we have done some benchmarking to ascertain that the spin state ordering is correct and that other spin states are unimportant.[15,16,44,45]

Cyclohexane Hydroxylation Catalyzed by $[(L)Fe^{IV}{=}O(OH)]^{+}$. The two isomers of $[(L)Fe^{IV}(O)(OH)]^{+}$ (see Figure 1), with the ferryl oxygen trans to N7 ($1_{transN7}$) or trans to N3 ($1_{transN3}$), were optimized in the intermediate-spin (S = 1) and high-spin (S = 2) electronic configurations. The isomer with the ferryl oxygen trans to N7 ($1_{transN7}$) is calculated to be slightly more stable than the trans to N3 geometry, but the energy difference of only 2 kJ/mol is not significant. The energy gap between the two electronic configurations with the high-spin state lower in energy by 20−30 kJ/mol is significant and as expected on the basis of an earlier investigation.[44] The key geometric parameters with Fe−N7 considerably longer than Fe−N3 and the bonds to the in-plane pyridine groups are as expected[46] and are listed together with the relative energies in Table 2.

TABLE 2: Selected Geometric Parameters (Bond Distances in Angstroms) and Spin Densities for $1_{transN7}$ and $1_{transN3}$ in the S = 2 and S = 1 Spin States; Relative Energies in Kilojoules per Mole

	Fe−N7	Fe−N3	Fe−O1	Fe−O2	S(Fe)	S(O1)	S(O2)	ΔE (kJ/mol)
			$[(L)Fe^{IV}{=}O(OH)]^{+}$ $1_{transN7}$					
S = 2	2.30	2.23	1.65	1.83	3.0	0.66	0.17	+0.0
S = 1	2.34	2.08	1.65	1.88	1.23	0.86	−0.06	+33.7
			$[(L)Fe^{IV}{=}O(OH)]^{+}$ $1_{transN3}$					
S = 2	2.33	2.18	1.83	1.65	3.02	0.17	0.63	+2.2
S = 1	2.28	2.11	1.88	1.65	1.28	0.83	−0.09	+23.9

The assumed mechanism is shown in Figure 2. We first concentrate on the activity of $[(L)Fe^{IV}{=}O(OH)]^{+}$; that of the corresponding Fe^{V} catalyst system will be discussed later. The stability and reactivity of the Fe^{IV} species was examined for both isomers ($1_{transN7}$ and $1_{transN3}$) in both spin states each (S = 1 and S = 2). All energies are quoted relative to the S = 2 ground state for both isomers. The hydrogen abstraction and subsequent rebound steps were modeled by a stepwise variation of the H−O1 and C−O1 distances.

The computed energy profile of the two reaction steps relative to the $1_{transN7}$ species in the S = 2 spin ground state is shown in Figure 3 (detailed geometries and spin densities of all species involved are given as Supporting Information). One of the axial hydrogen atoms of cyclohexane is transferred to the ferryl oxygen atom to yield an Fe^{III} intermediate and an alkyl radical (rad). On the S = 2 spin surface, this step is associated with a linear transition state (*ts1*; E = +47.8 kJ/mol; C−H−O angle of 174.8 Å, Fe−O−H angle of 175.0 Å; see Figure 4; linear Fe−O···H···R transition states on quintet surfaces were found before[47]). Similar to $1_{transN7}$, the computed geometry of *ts1* has a significantly elongated Fe−N7 bond (2.60 Å). Formally, the hydrogen abstraction reduces the Fe^{IV} center to Fe^{III} (one electron from the corresponding cyclohexane carbon atom is transferred to the iron center), and this also emerges from the calculated spin densities of *ts1* (S(Fe = 3.78, S(O1) = 0.13, S(O2) = 0.29, see Figure 4). *ts1* decays to the radical intermediate *rad*, where the unpaired electron of the cyclohexyl carbon atom couples with the five d electrons of the Fe^{III} center; ferromagnetic and antiferromagnetic coupling lead to a heptet (rad_{heptet}, E = +1.2 kJ/mol, S(Fe) = 3.97, S(C) = 0.99) and a quintet state ($rad_{quintet}$, E = +0.4 kJ/mol, S(Fe) = 3.96, S(C) = −0.95), respectively (see Supporting Information for structural parameters). The rebound step was modeled by a stepwise variation of the C−O distance. A transition state was found on the heptet surface (*ts2*, E = +103.2 kJ/mol, S(Fe) = 4.06, S(O1) = 0.17, S(O2) = 0.36, S(C) = 0.42), which is +55.4 kJ/mol higher than the hydrogen abstraction transition state, *ts1* (see Figure 3). The spin density analysis shows that the radical electron is approaching the Fe^{III} center, and this eventually yields the Fe^{II} rebound product species. The heptet surface is expected to produce the rebound product (E = +7.6 kJ/mol) with six unpaired electrons (S = 3). Therefore, the modeled rebound product on this surface is associated with spin densities of 4.05 for Fe, and the remaining spin density is delocalized over the coordinated donor atoms. In contrast to the radical intermediate on the heptet surface (rad_{heptet}), the $rad_{quintet}$ intermediate, which is slightly lower in energy (effectively, the two spin states are degenerate, see Figure 3) directly leads in a barrier-less reaction to the rebound product (E = −187.0 kJ/mol, S(Fe) = 3.69) in the electronic ground state (S = 2).

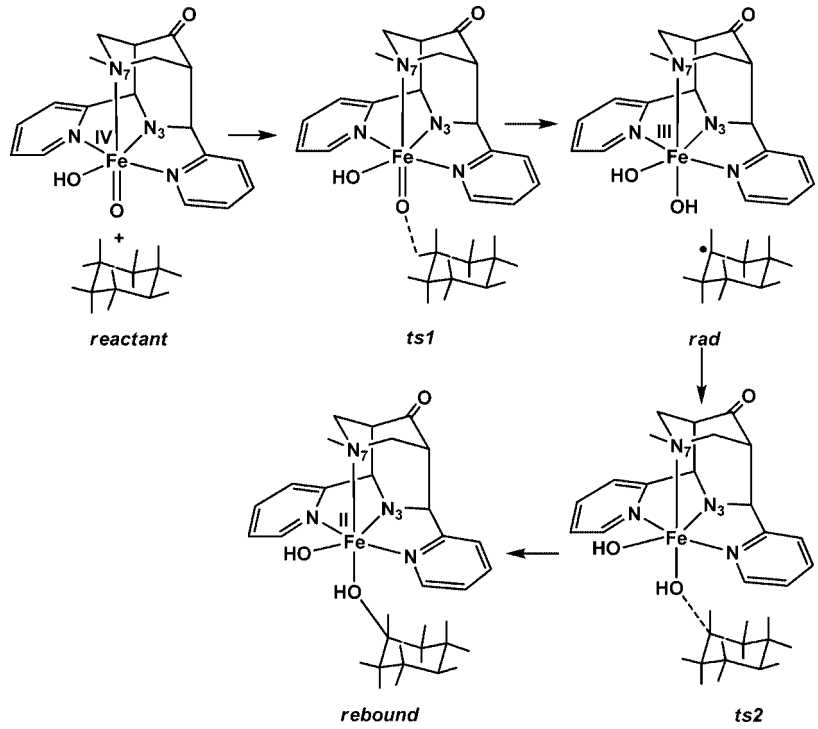

Figure 2. Assumed mechanism for the cyclohexane hydroxylation by $[(L)Fe^{IV}{=}O(OH)]^{+}$ (the same mechanistic pathway was used for $[(L)Fe^{V}{=}O(OH)]^{2+}$).

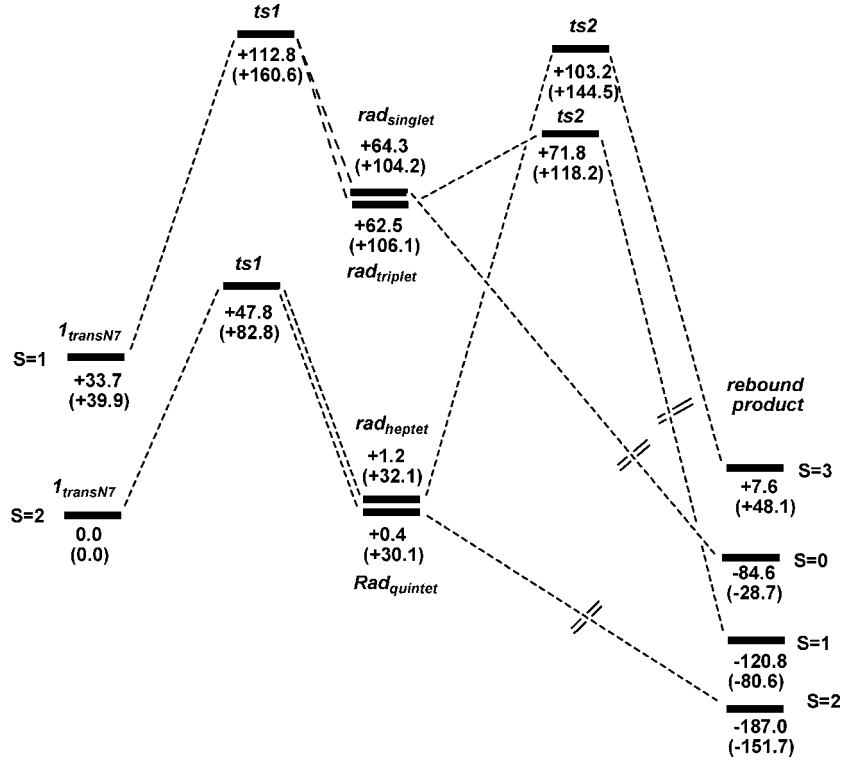

Figure 3. Cyclohexane hydroxylation catalyzed by $[(L)Fe^{IV}{=}O(OH)]^{+}$, $1_{transN7}$ (energies in kilojoules per mole, free energies in parenthesis).

The S = 1 spin surface was also modeled, and the results are included in Figures 3 and 4. The main structural differences between the two spin surface are related to the Fe−N7 distances: in the S = 1 spin state, the Fe−N7 bond is comparably short (2.31 vs 2.60 Å, see Figure 4), and this is due to subtle effects related to a the combination of the trans influence excerted by OH^{-} and Jahn−Teller-type effects on the high spin surface.[44] The geometric differences are also reflected in the energies, and as a result, the hydrogen abstraction step on the intermediate-spin surface is found to have a high barrier (E = +112.8 kJ/mol), 65.0 kJ/mol higher than for the S = 2 pathway. Another possible reason for the exceedingly high energy barrier is the geometry of *ts1*, which has longer C−H (1.33 Å) and shorter O−H distances (1.22 Å) compared with those on the S = 2 surface (late vs early transition state). The rebound transition state *ts2* on the triplet surface is lower in energy by 31.4 kJ/mol less than that found on the heptet surface (*ts2*, E = 71.8 kJ/mol). Consistent with

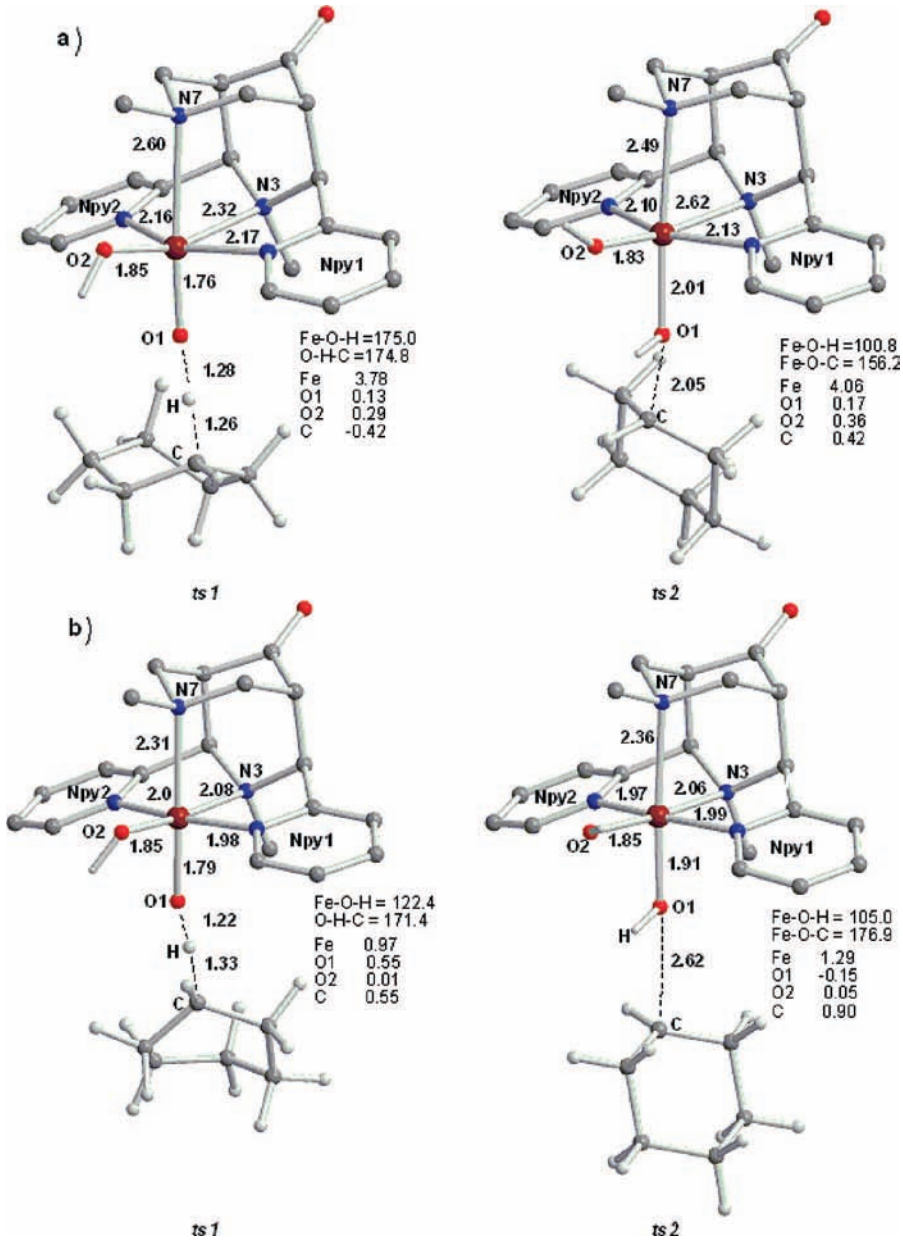

Figure 4. (a) Transition states for hydrogen abstraction and rebound steps for $1_{transN7}$ on the S = 2 surface; (b) the corresponding transition states on the S = 1 surface.

the $rad_{quintet}$ intermediate, the $rad_{singlet}$ species directly yields the rebound product in a barrier-less process.

The combined analysis of S = 2 and S = 1 pathways suggest that the oxidation of cyclohexane preferably occurs on the high-spin surface (S = 2). This is as expected from studies with other systems.[48−50] The rebound step is barrier-less on the quintet surface, and the two spin states of the intermediate (rad_{heptet} and $rad_{quintet}$) are almost degenerate. Therefore, the initial rad_{heptet} species can readily interchange to $rad_{quintet}$, to yield in a barrier-less second step, the thermodynamically most favorable product. Overall, the S = 2 pathway is associated with activation and reaction energies of +47.8 and −187.0 kJ/mol, respectively. As the degree of disorder decreases along the pathway, the effect of entropy is destabilizing (approximately (+30)−(+40) kJ/mol) on both spin surfaces.

Both S = 1 and S = 2 spin states were also modeled for the other possible isomer, $1_{transN3}$ (see Figure 5). As expected, here also the S = 2 spin state is more stable (by +21.7 kJ/mol). The hydrogen abstraction on this spin surface occurs with a low energy barrier (*ts1*, E = +23.2 kJ/mol), 24.6 kJ/mol lower in energy than that for the $1_{transN7}$ isomer. The hydrogen abstraction leads to the formation of the radical intermediate, where the heptet (rad_{heptet}; E = −19.9 kJ/mol, C−H = 2.16 Å) and quintet states ($rad_{quintet}$; E = −21.4 kJ/mol, C−H = 2.04 Å) are close to degenerate. Here again, the heptet surface is associated with a high energy transition state (*ts2*, E = +102.1 kJ/mol; S(Fe) = 4.05, S(O1) = 0.18, S(O2) = 0.39, S(C) = 0.40), while the quintet surface has no transition state for the rebound step. Similar to $1_{transN7}$, the rebound step on the heptet surface has a higher activation energy by 78.9 kJ/mol more than the initial hydrogen abstraction step, and the rebound product with 6 and 4 unpaired electrons is formed with energies of +33.0 and −171.8 kJ/mol, respectively. Consistent with the results of the $1_{transN7}$ isomer, the hydrogen abstraction step on the S = 1 spin surface is associated with a higher energy barrier (by +70.8 kJ/mol) more than that of the S = 2 pathway. In the subsequent rebound step, the triplet surface has a barrier of 86.0 kJ/mol,

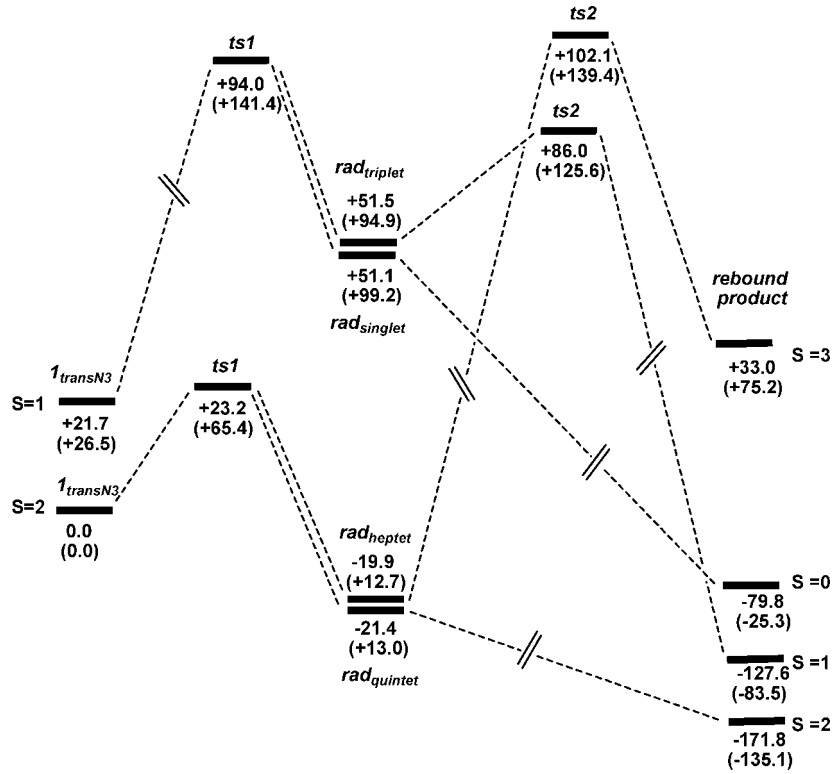

Figure 5. Cyclohexane hydroxylation catalyzed by $[(L)Fe^{IV}{=}O(OH)]^+$, $1_{transN3}$ (energies in kilojoules per mole, free energies in parenthesis).

TABLE 3: Activation and Reaction Energies (Kilojoules per Mole) of $[(L)Fe^{IV}{=}O(OH)]^+$ on the S = 2 Surface

complex	$\Delta E^{\ddagger}$	$\Delta G^{\ddagger}$	$\Delta E_{R.E}$	$\Delta G_{R.E}$
$1_{transN7}$	+47.8	+82.8	−187.0	−151.7
$1_{transN3}$	+23.2	+65.4	−171.8	−135.1

and the reaction on the singlet surface is barrier-less. The overall trends for both isomers $1_{transN3}$ and $1_{transN7}$ are very similar.

The activation and reaction energies of $1_{transN7}$ and $1_{transN3}$ on the S = 2 spin surface are listed in Table 3. As discussed above, entropy effects in general lead to a destabilization of the transition states, intermediates, and products. However, the entropy contributions are similar for both isomers. $1_{transN3}$ has a lower activation energy than the slightly more stable $1_{transN7}$ isomer; the overall reaction is slightly more exothermic for $1_{transN7}$ than for $1_{transN3}$, but the energy differences are generally small. It emerges that the system $1_{transN3}/1_{transN7}$ is an efficient catalyst for the cyclohexane hydroxylation.

Cyclohexane Hydroxylation Catalyzed by $[(L)Fe^{V}{=}O(OH)]^{2+}$. From the different reactivities of the system with H_2O_2 and PhIO as oxidant (see above and Table 1) it appears that various pathways are involved, possibly including $Fe^{IV}{=}O$ as well as $Fe^{V}{=}O$ and radical intermediates of variable lifetime. However, the limited amount of experimental data does not allow an unambiguous assignment of the oxidation state of the catalytically active species. Therefore, the activity of $[(L)Fe^{V}{=}O(OH)]^{2+}$ was also examined and compared with the corresponding Fe^{IV} system. Similar to $[(L)Fe^{IV}{=}O(OH)]+$, the isomers of $[(L)Fe^{V}{=}O(OH)]^{2+}$ ($2_{transN7}$ and $2_{transN3}$) were modeled with the two possible spin states, S = 3/2 and S = 1/2. The metal-donor bonds of $[(L)Fe^{V}{=}O(OH)]^{2+}$ are, as expected, in general slightly shorter than those of the corresponding Fe^{IV} complex (see Tables 2 and 4). The most significant differences occur in the Fe−N7 and Fe−N3 distances, which are 0.1−0.2 Å shorter than those in $[(L)Fe^{IV}{=}O(OH)]^+$. For both isomers ($2_{transN7}$ and $2_{transN3}$), the

TABLE 4: Selected Geometric Parameters (Bond Distances in Angstroms) and Spin Densities for $2_{transN7}$ and $2_{transN3}$ in the S = 3/2 and S = 1/2 Spin States; Relative Energies in Kilojoules per Mole

	Fe−N7	Fe−N3	Fe−O1	Fe−O2	S(Fe)	S(O1)	S(O2)	ΔE (kJ/mol)
				$[(L)Fe^{V}{=}O(OH)]^{2+}$ $2_{transN7}$				
S = 3/2	2.25	2.05	1.67	1.79	1.69	1.13	0.28	+3.3
S = 1/2	2.23	2.04	1.69	1.79	0.12	1.32	−0.42	+49.3
				$[(L)Fe^{V}{=}O(OH)]^{2+}$ $2_{transN3}$				
S = 3/2	2.23	2.06	1.80	1.67	1.79	1.09	0.24	+0.0
S = 1/2	2.19	2.05	1.80	1.68	0.19	1.26	−0.48	+49.6

S = 3/2 spin state is found to be the ground state, and this is stabilized by +45.9 kJ/mol and +49.6 kJ/mol, respectively.

Figures 7 and 8 show the computed pathways for the cyclohexane hydroxylation by the two isomers of $[(L)Fe^{V}{=}O(OH)]^{2+}$, $2_{transN7}$ and $2_{transN3}$; geometric parameters of the computed structures are given in Figures 7 and 8 and in Table 5. The behavior of the two Fe^{V} complexes is very different from that of the corresponding Fe^{IV} catalysts. For $2_{transN7}$ and $2_{transN3}$, the hydrogen abstraction directly leads to the rebound product, without forming a radical intermediate. The spin densities on *ts1* ($2_{transN7}$: S(Fe) = 1.69, S(O1) = 0.73, S(O2) = 0.21, S(C) = 0.37; $2_{transN3}$: S(Fe) = 2.73, S(O1) = 0.06, S(O2) = 0.61, S(C) = −0.09) show some radical character on the carbon atoms, but these do not decay into radical intermediates and instead directly lead to the rebound products. For $2_{transN7}$, *ts1* is computed to have an energy barrier of 11.9 kJ/mol, and this is 35.9 kJ/mol lower than that for $1_{transN7}$ on the prefered S = 2 spin surface. This is probably due to the early transition state *ts1* (C−H = 1.25 Å, O1−H = 1.36 Å) in $2_{transN7}$, where the C−H distance is 0.01 Å shorter and the O1−H distance is 0.08 Å longer than in *ts1* of the Fe^{IV} catalyst $1_{transN7}$. The situation for the isomer $2_{transN3}$ is very similar, with the shorter C−H distance (1.14 Å) and longer O2−H distance (1.80 Å) compared with that in $1_{transN3}$. A comparison of Figures 7 and 8 indicates

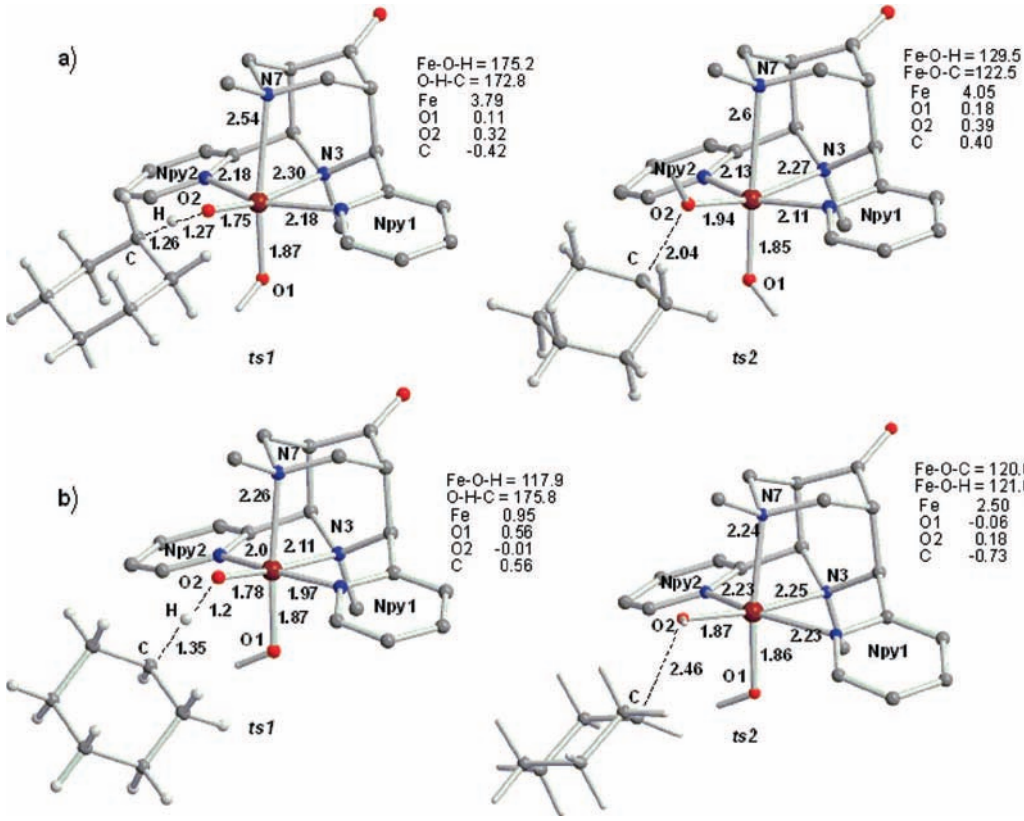

Figure 6. (a) Transition states for hydrogen abstraction and rebound steps for $1_{transN3}$ on the S = 2 surface. (b) Transition states for hydrogen abstraction and rebound steps for $1_{transN3}$ on the S = 1 surface.

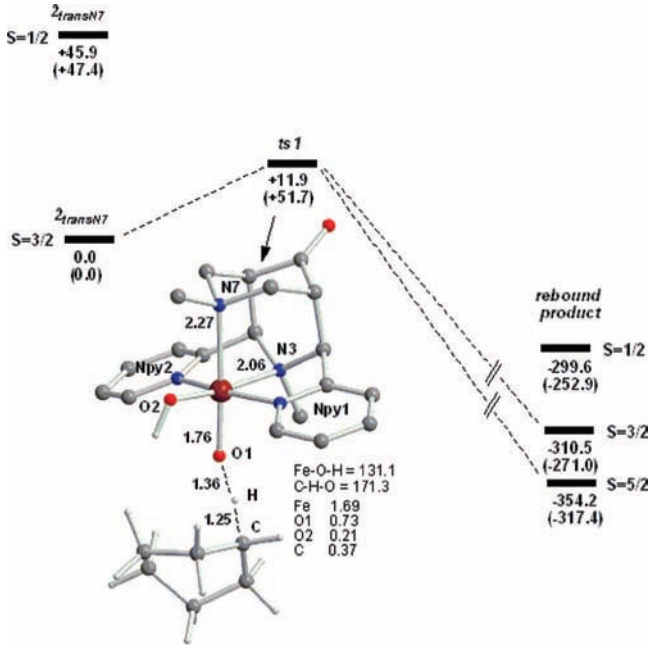

Figure 7. Cyclohexane hydroxylation catalyzed by $[(L)Fe^{V}{=}O(OH)]^{2+}$, $2_{transN7}$ (energies in kilojoules per mole, free energies in parenthesis).

that the more stable isomer $2_{transN3}$ is associated with a lower activation energy ($\Delta E^{\ddagger}$ = +0.4 vs 11.9 kJ/mol, $\Delta G^{\ddagger}$ = +39.3 vs 51.7 kJ/mol), but the overall reaction is thermodynamically less favorable by over 20 kJ/mol than for $2_{transN7}$. This is consistent with the results obtained for the catalyst in the +IV oxidation state, $1_{transN3}$ versus $1_{transN7}$.

Interestingly, the S = 1/2 spin state for $2_{transN7}$ has a very flat potential energy surface with a small barrier of +3.2 kJ/mol for hydrogen abstraction (no transition state was found for $2_{transN3}$). Inclusion of zero point corrections further stabilizes the transition state; that is, the barrier on the S = 1/2 spin surface is extremely flat. Therefore, a spin transition to the S = 1/2 surface may occur before the transition state *ts1*. However, the reactant on the S = 1/2 surface is very high in energy (+46 kJ/mol). Therefore, a spin transition is very difficult, and the reaction probably occurs on the S = 3/2 spin surface. The rebound products with S = 5/2, 3/2, and 1/2 spin states were computed, and the one with S = 5/2 is the most stable (E = −354.2 kJ/mol, see Table 5).

TABLE 5: Selected Geometric Parameters (Bond Distances in Angstroms) and Spin Densities for the Rebound Products of $2_{transN7}$ and $2_{transN3}$ in the S = 5/2, 3/2 and 1/2 Spin States

	Fe−N7	Fe−N3	Fe−O1	Fe−O2	S(Fe)	S(O1)	S(O2)
rebound products for $2_{transN7}$							
S = 5/2	2.36	2.25	2.16	1.79	4.03	0.06	0.44
S = 3/2	2.39	2.06	2.32	1.78	2.75	0.03	0.19
S = 1/2	2.15	2.07	2.06	1.80	0.90	−0.01	0.17
rebound products for $2_{transN3}$							
S = 5/2	2.47	2.22	1.80	2.09	4.01	0.47	0.07
S = 3/2	2.22	2.23	1.81	2.16	2.85	0.02	0.05
S = 1/2	2.24	2.01	1.81	2.05	0.94	0.15	0.00

Comparison of the Pathways Involving $[(L)Fe^{IV}{=}O(OH)]^{+}$ and $[(L)Fe^{V}{=}O(OH)]^{2+}$ (1 and 2). The data discussed so far indicate that cyclohexane hydroxylation for both oxidation states of the catalyst preferably occurs via the O trans to N3 isomer on the high-spin surfaces, $[(L)Fe^{IV}{=}O(OH)]^{+}$ (S = 2) and $[(L)Fe^{V}{=}O(OH)]^{2+}$ (S = 3/2). The corresponding pathways will now be compared with each other. Table 6 shows that $[(L)Fe^{V}{=}O(OH)]^{2+}$ ($2_{transN3}$) has a very low activation energy barrier for cyclohexane hydroxylation (the barrier $\Delta E^{\ddagger}_2$ for $1_{transN3}$ is larger by over 20 kJ/mol). The same trend is seen for

TABLE 6: Activation and Reaction Energies of $[(L)Fe^{IV}{=}O(OH)]^+$ $1_{transN3}$ and $[(L)Fe^{V}{=}O(OH)]^{2+}$ $2_{transN3}$; Energies in Kilojoules per Mole

complex	$\Delta E^{\ddagger}$	$\Delta G^{\ddagger}$	$\Delta E_{R.E}$	$\Delta G_{R.E}$
$1_{transN3}$	+23.2	+65.4	−171.8	−135.1
$2_{transN3}$	+0.4	+39.3	−332.8	−296.3

TABLE 7: Activation and Reaction Energy for the Oxidation of $[(L)Fe^{II}(NCCH_3)_2]^{2+}$ (S = 2); Energies in Kilojoules per Mole

Pathways	$\Delta E^{\ddagger}$	$\Delta G^{\ddagger}$	$\Delta E_{R.E}$	$\Delta G_{R.E}$
$[(L)Fe^{II}(NCCH_3)_2]^{2+} \rightarrow$ $1_{transN3}$ (S = 2)	+224.1	+186.8	+69.5	+34.6
$[(L)Fe^{II}(NCCH_3)_2]^{2+} \rightarrow$ $2_{transN3}$ (S = 3/2)	+222.9	+164.4	+148.8	+89.7
$[(L)Fe^{II}(NCCH_3)_2]^{2+} \rightarrow$ $3_{transN3}$ (S = 2)	+223.8	+200.5	+30.2	−5.05

the free energy of activation. In addition, the rebound product in its electronic ground state is thermodynamically more stable on the Fe^{V}- than on the Fe^{IV}-catalyzed pathway. Alltogether, the energetics suggest that $[(L)Fe^{V}{=}O(OH)]^{2+}$, $2_{transN3}$, is catalytically more active than $[(L)Fe^{IV}{=}O(OH)]^{+}$, $1_{transN3}$.

However, the preferred pathway also depends on the accessibility of the catalytically active species with respect to the precatalyst, $[(L)Fe^{II}(NCCH_3)_2]^{2+}$ (the species involved in the catalytic cycle for the Fe^{II}/Fe^{IV} system are given in Figure 2, for the Fe^{III}/Fe^{V} cycle the corresponding species all have a +1 higher charge). A detailed DFT study (B3LYP/TZVPP) of the oxidation of $[(L)Fe^{II}(NCCH_3)_2]^{2+}$ by H_2O_2 has been carried out, and three different pathways have been considered: $[(L)Fe^{II}(H_2O_2)(NCCH_3)]^{2+}$ (S = 2) to produce $[(L)Fe^{IV}{=}O(OH)]+$ (S = 2), $1_{transN3}$, $[(L)Fe^{V}{=}O(OH)]^{2+}$ (S = 3/2), $2_{transN3}$, and $[(L)Fe^{IV}{=}O(OH_2)]^{2+}$ (S = 2), $3_{transN3}$.[51] The energies for the transformation of the Fe^{II} precatalyst to the putative active forms have been recalculated at the B3LYP/LACV3p++** level. Table 7 shows the activation and reaction energies for the production of $1_{transN3}$, $2_{transN3}$, and $3_{transN3}$. All three pathways involve similar activation enthalpies (approximately 220 kJ/mol); that is, it is impossible to derive any kinetic preference from these data. However, the free energy corrections reduce the activation barrier for $2_{transN3}$ (the Fe^{V} species) to a more than 20 or nearly 40 kJ/mol lower value than for the other two pathways. With respect to the thermodynamic stability, the Fe^{IV} catalysts are preferred by at least 50 kJ/mol. From Table 7, it follows that entropy plays an important role, especially in the case of $2_{transN3}$. Kinetically, the reaction from $[(L)Fe^{II}(NCCH_3)_2]^{2+}$ to $2_{transN3}$ is favored compared with those forming $1_{transN3}$ and $3_{transN3}$. Thermodynamically, it is uphill by +55.1 kJ/mol and +94.7 kJ/mol compared with $1_{transN3}$ and $3_{transN3}$, respectively.[52]

Conclusion

Thermodynamically, the Fe^{IV} complexes are more stable than the Fe^{V} catalysts (by about 50 kJ/mol, see Table 7). However, the activation barriers from the Fe^{II} precatalysts are smaller for the Fe^{V} complex by approximately 20 kJ/mol (see Table 7). The barriers for C−H activation for both oxidation states are smaller (65 kJ/mol for Fe^{IV} and 40 kJ/mol for Fe^{V}) than the back reactions (150 and 70 kJ/mol, respectively; see Tables 3, 6, and 7). From the computed data, it therefore appears that both $[(L)Fe^{IV}{=}O(OH)]^{+}$ and $[(L)Fe^{V}{=}O(OH)]^{2+}$ (and also $[(L)Fe^{IV}{=}O(OH_2)]^{2+}$, depending on the solvent and the acidity of the solution; the trans to N3 isomers in all cases) are efficient

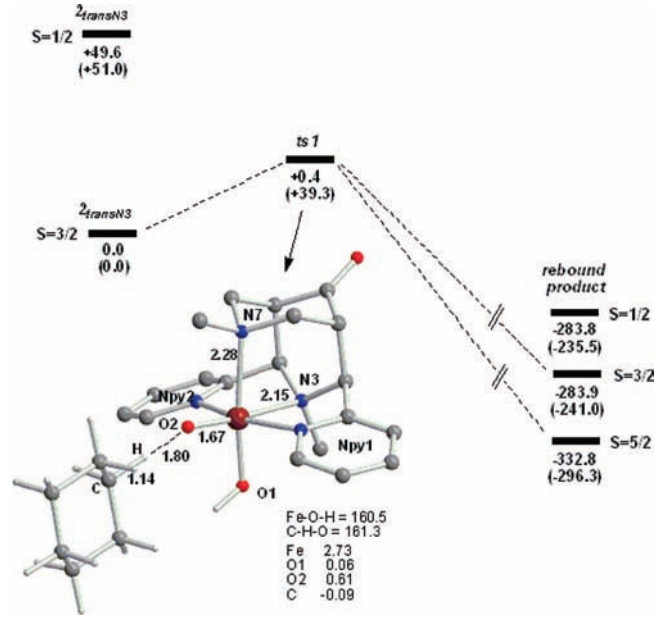

Figure 8. Cyclohexane hydroxylation catalyzed by $[(L)Fe^{V}{=}O(OH)]^{2+}$, $2_{transN3}$ (energies in kilojoules per mole, free energies in parenthesis).

catalysts for C−H activation and oxygen transfer. On the basis of the present data and including error limits of up to 10−20 kJ/mol[53] and appreciable solvent effects,[15] the two pathways may compete. And this is exactly what the experiments suggested. The Fe^{IV} route, enforced by a stoichiometric reaction with PhIO as oxidant, seem to involve cyclohexyl radicals of a significant lifetime, while this does not seem to be the case in the H_2O_2-initiated reaction, which might involve $Fe^{V}{=}O$ as the catalytically active species.

Acknowledgment. We are grateful for generous financial support by the German Science Foundation (DFG).

Supporting Information Available: Detailed geometries and spin densities of all species involved and structural parameters. This material is available free of charge via the Internet at http://pubs.acs.org.

References and Notes

(1) Costas, M.; Mehn, M. P.; Jensen, M. P.; Que Jr., L. *Chem. Rev.* **2004**, *104*, 939.
(2) Solomon, E. I.; Brunold, T. C.; Davis, M. I.; Kensley, J. N.; Lee, S.-K.; Lehnert, N.; Neese, F.; Skulan, A. J.; Yang, Y.-S.; Zhou, J. *Chem. Rev.* **2000**, *100*, 235.
(3) Nordlund, P. *Handbook of Metalloproteins*; Bertini, I., Sigel, A., Sigel, H., Eds.; Marc Dekker: New York, 2001; pp 461.
(4) Nam, W. *Acc. Chem. Res.* **2007**, *40*, 522.
(5) Bassan, A.; Blomberg, M. R. A.; Siegbahn, P. E. M.; Que Jr., L. *Chem. Eur. J.* **2005**, *11*, 692.
(6) Chen, K.; Que, L. *J. Am. Chem. Soc.* **2001**, *123*, 6327.
(7) Kaiser, J.; Klinker, E. J.; Oh, N. Y.; Rohde, J.-U.; Song, W. J.; Stubna, A.; Kim, J.; Münck, E.; Nam, W.; Jr, L. Q. *J. Am. Chem.Soc.* **2004**, *126*, 472.
(8) Barton, D. H. R.; Doller, D. *Acc. Chem. Res.* **1992**, *25*, 504.
(9) Barton, D. H. R. *Tetrahedron* **1998**, *54*, 6805.
(10) Barton, D. H. R. *Tetrahedron* **1998**, *54*, 1735.
(11) Rohde, J.-U.; In, J.-H.; Lim, M. H.; Brennessel, W. W.; Bukowski, M. R.; Stubna, A.; Münck, E.; Nam, W.; Que Jr., L. *Science* **2003**, *299*, 1037.
(12) Price, J. C.; Barr, E. W.; Glass, T. E.; Krebs, C.; Bollinger Jr., M. *J. Am. Chem. Soc.* **2003**, *125*, 13008.
(13) Price, J. C.; Barr, E. W.; Tirupati, B.; Bollinger Jr., M.; Krebs, C. *Biochemistry* **2003**, *42*, 7497.
(14) Bassan, A.; Blomberg, M. R. A.; Siegbahn, P. E. M.; Que, J. L. *J. Am. Chem. Soc.* **2002**, *124*, 11056.

(15) Comba, P.; Rajaraman, G.; Rohwer, H. *Inorg. Chem.* **2007**, *46*, 3826.
(16) Bautz, J.; Comba, P.; Lopez de Laorden, C.; Menzel, M.; Rajaraman, G. *Angew. Chem., Int. Ed.* **2007**, *46*, 8067.
(17) Priestley, N. D.; Floss, H. G.; Froland, W. A.; Lipscomb, J. D.; Williams, P. G.; Morimoto, H. *J. Am. Chem. Soc.* **1992**, *114*, 7561.
(18) Valentine, A. M.; Wilkinson, B.; Liu, K. E.; Komar-Panicucci, S.; Priestley, N. D.; Williams, P. G.; Morimoto, H.; Floss, H. G.; Lippard, S. J. *J. Am. Chem. Soc.* **1997**, *119*, 1818.
(19) Stubbe, J.; Kozarich, J. W. *Chem. Rev.* **1987**, *87*, 1107.
(20) McGall, G. H.; Rabow, L. E.; Stubbe, J.; Kozarich, J. W. *J. Am. Chem. Soc.* **1987**, *109*, 1836.
(21) Rabow, L. E.; McGall, G. H.; Stubbe, J.; Kozarich, J. W. *J. Am. Chem. Soc.* **1990**, *112*, 3203.
(22) Ingold, K. U. MacFaul, P. A., (Ed. Meunier, B.), *Biomimetic Oxidations Catalyzed by Transition Metal Complexes*, World Scientific Publishing and Imperial College Press: London, 2000.
(23) Russel, G. A. *J. Am. Chem.Soc.* **1957**, *79*, 3871.
(24) Groves, J. T. *J. Chem. Educ.* **1985**, *62*, 928.
(25) Bowry, V. W.; Ingold, K. U. *J. Am. Chem.Soc.* **1991**, *113*, 5699.
(26) Newcomb, M.; Tadic-Biadatti, M.-H. L.; Chestney, D. L.; Roberts, E. S.; Hollenberg, P. F. *J. Am. Chem. Soc.* **1995**, *117*, 12085.
(27) Kim, C.; Chen, K.; Kim, J.; Que Jr., L. *J. Am. Chem. Soc.* **1997**, *119*, 5964.
(28) Chen, K.; Que, J. L. *J. Chem. Soc., Chem. Commun.* **1999**, 1375.
(29) Lubben, M.; Meetsma, A.; Wilkinson, E. C.; Feringa, B.; Que, J. *Angew. Chem., Int. Ed.* **1995**, *34*, 1512.
(30) Roelfes, G.; Lubben, M.; Chen, K.; Ho, R. Y. N.; Meetsma, A.; Genseberger, S.; Hermant, R. M.; Hage, R.; Mandal, S. K.; Young Jr., V. G.; Zang, Y.; Kooijman, H.; Spek, A. L.; Que Jr, L.; Feringa, B. L. *Inorg. Chem.* **1999**, *38*, 1929.
(31) Börzel, H.; Comba, P.; Hagen, K. S.; Merz, M.; Lampeka, Y. D.; Lienke, A.; Linti, G.; Pritzkow, H.; Tsymbal, L. V. *Inorg. Chim. Acta* **2002**, *337*, 407.
(32) Schrödinger, JAGUAR 6.5; Schrödinger LLC: New York, 2005.
(33) Becke, A. D. *J. Chem. Phys.* **1992**, *96*, 2155.
(34) Becke, A. D. *J. Chem. Phys.* **1992**, *97*, 9713.
(35) Becke, A. D. *J. Chem. Phys. B* **1993**, *98*, 5648.
(36) Hay, J. P.; Wadt, W. R. *J. Chem. Phys.* **1985**, *82*, 99.
(37) Friesner, R. A.; Murphy, R. B.; Beachy, M. D.; Ringlanda, M. N.; Pollard, W. T.; Dunietz, B. D.; Cao, Y. X. *J. Phys. Chem. A.* **1999**, *103*, 1913.
(38) Hasman, D.; Beachy, M. D.; Wang, L.; Friesner, R. A. *J. Comput. Chem.* **1998**, *19*, 1017.
(39) Frisch, M. J.; Trucks, G. W.; Schlegel, H. B.; Scuseria, G. E.; Robb, M. A.; Cheeseman, J. R. ; Montgomery J. A., Jr.; Vreven, T.; Kudin, K. N.; Burant, J.C.; Millam, J. M.; Iyengar, S. S.; Tomasi, J.; Barone, V.; Mennucci, B.; Cossi, M.; Scalmani, G.; Rega, N.; Petersson, G. A.; Nakatsuji, H.; Hada, M.; Ehara, M.; Toyota, K.; Fukuda, R.; Hasegawa, J.; Ishida, M.; Nakajima, T.; Honda, Y.; Kitao, O.; Nakai, H.; Klene, M.; Li, X.; Knox, J. E.; Hratchian, H. P.; Cross, J. B.; Bakken, V.; Adamo, C.; Jaramillo, J.; Gomperts, R.; Stratmann, R. E.; Yazyev, O.; Austin, A. J.; Cammi, R.; Pomelli, C.; Ochterski, J. W.; Ayala, P. Y.; Morokuma, K.; Voth, G. A.; Salvador, P.; Dannenberg, J. J.; Zakrzewski, V. G.; Dapprich, S.; Daniels, A. D.; Strain, M. C.; Farkas, O.; Malick, D. K.; Rabuck, A. D.; Raghavachari, K.; Foresman, J. B.; Ortiz, J. V.; Cui, Q.; Baboul, A. G.; Clifford, S.; Cioslowski, J.; Stefanov, B. B.; Liu, G.; Liashenko, A.; Piskorz, P.; Komaromi, I.; Martin, R. L.; Fox, D. J.; Keith, T.; Al.Laham, M. A.; Peng, C. Y.; Nanayakkara, A.; Challacombe, M.; Gill, P. M. W.; Johnson, B.; Chen, W.; Wong, M. W.; Gonzalez, C.; Pople, J. A. *Gaussian 03, Revision C.02*; Gaussian, Inc.: Wallingford CT, 2004.
(40) Cancès, M. T.; Mennucci, B.; Tomasi, J. *J. Chem. Phys.* **1997**, *107*, 3032.
(41) Cossi, M.; Barone, B.; Mennucci, B.; Tomasi, J. *Chem. Phys. Lett.* **1998**, *286*, 253.
(42) Mennucci, B.; Tomasi, J. *J. Chem. Phys.* **1997**, *106*, 5151.
(43) Cossi, M.; Scalmani, G.; Raga, N.; Barone, V. *J. Chem. Phys.* **2002**, *117*, 43.
(44) Anastasi, A.; Comba, P.; McGrady, J.; Lienke, A.; Rohwer, H. *Inorg. Chem.* **2007**, *46*, 6420.
(45) Comba, P.; Rajaraman, G. *Inorg. Chem.* **2008**, *47*, 78.
(46) Bukowski, M. R.; Comba, P.; Limberg, C.; Merz, M.; Que Jr, L.; Wistuba, T. *Angew. Chem., Int. Ed.* **2004**, *43*, 1283.
(47) De Visser, S. P. *J. Am. Chem. Soc.* **2006**, *128*, 8590.
(48) Hirao, H.; Kumar, D.; Que, L. J.; Shaik, S. *J. Am. Chem. Soc.* **2006**, *128*, 8590.
(49) De Visser, S. P. *J. Am. Chem. Soc.* **2006**, *128*, 9813.
(50) De Visser, S. P.; Oh, K.; Han, A.-R.; Nam, W. *Inorg. Chem.* **2007**, *46*, 4632.
(51) In ref 12, the overall reaction, for example, Fe^{II} leading to Fe^{V}, has been broken down into several steps, such as the substitution of MeCN by H_2O_2. Each step was treated individually, and the corresponding entropy effects were included. Therefore, the reference energy was changing for each step. For modeling entire reaction pathways, this is not an appropriate approach. In the current study, for the formation of $1_{transN3}$, $2_{transN3}$, and $3_{transN3}$, the reference point for all free energy and enthalpy terms is $[(L)Fe^{II}(NCCH_3)_2]^{2+}$.
(52) Note that, so far, we have not discussed in detail the reactivity of $3_{transN3}$ and $3_{transN7}$ with respect to the cyclohexane oxygenation reaction. It appears that the $3_{transN3}$ isomer is the more likely one to be involved in the oxygen transfer reaction and that its reactivity is similar to that of the corresponding hydroxo complex $1_{transN3}$ but with a somewhat smaller activation barrier. Details are given as Supporting Information.
(53) Siegbahn, P. E. M. *J. Comput. Chem.* **2001**, *22*, 1634.

JP8037895